J. Fluid Mech. (1983), *vol.* 127, *pp.* 403–428
Printed in Great Britain

Laterally converging flow. Part 2. Temporal wall shear stress

By F. W. CHAMBERS†,
University of New Mexico, Albuquerque, NM 87131
H. D. MURPHY
Los Alamos National Laboratory, Los Alamos, NM 87545
AND D. M. McELIGOT
University of Arizona, Tucson, AZ 85721

(Received 11 August 1981 and in revised form 5 May 1982)

Instantaneous measurements of the wall shear stress were made in the laterally converging duct also used for mean measurements in part 1 and were analysed by conditional sampling and by conditional averaging. The sidewalls of the duct were adjusted to provide (i) a straight duct of constant rectangular cross-section and (ii) laterally (spanwise) converging ducts resulting in streamwise acceleration of the flow. The Reynolds number varied from 7600 to 47200 and the dimensionless acceleration parameter $K_V = (\nu/V^2)\,dV/dx$ ranged from 0 to $3{\cdot}4 \times 10^{-6}$, yielding a variation of the flow regime from fully turbulent to nearly laminar. The typical burst pattern, or conditionally averaged time history of the wall shear stress, resembled the time history of the streamwise velocity component deduced at $y^+ = 15$ by Blackwelder and Kaplan using the same general technique. For fully developed flows, inner or wall scaling of the bursting frequency was found to be less dependent upon Reynolds number than outer scaling; other characteristics examined varied with both inner and outer scaling. For converging flows measurements of bursting characteristics essentially confirmed the indicated flow regimes deduced in part 1 and showed that the measured characteristic that was most affected by acceleration was the bursting frequency. All characteristics varied with acceleration, but the variation was generally less when normalized by wall variables rather than when normalized by outer variables.

1. Introduction

In the companion paper (part 1) by Murphy, Chambers & McEligot (1983), the flow state in a laterally converging duct was inferred from measurements of mean wall shear stresses, local pressure gradients and integral streamwise pressure differences. The present paper examines the correspondence between those observations and the turbulence structure, in particular the bursting phenomenon, via conditionally averaged measurements of the temporal wall shear-stress signal $\tau(t)$.‡ In the process, several important questions concerning bursting are answered.

The bursting phenomenon in the viscous layer has been described well by Corino

† Present address: Lockheed-Georgia Company, Marietta, GA 30063.

‡ Since the only shear stress measured in the present work is at the surface, the usual subscript w or 0 will be dropped from τ_w in the remainder of this paper.

& Brodkey (1969), Kline *et al.* (1967), Offen & Kline (1974) and others, as well as by recent reviews (Willmarth 1975; Cantwell 1981), so only the literature pertinent to the present study will be reviewed here. With Kim, Kline & Reynolds (1971) and Blackwelder & Kaplan (1976) we adopt the term 'bursting' or 'bursting phenomenon' for the overall process. For convenience in description, the phases of the process will be termed (*a*) a deceleration or ejection, (*b*) a rapid acceleration or sweep, and (*c*) a relatively quiescent process, or more gradual deceleration following the sweep. Blackwelder & Kaplan (1976) have demonstrated one version of the typical bursting signal by conditional averaging of the fluctuation in the streamwise velocity component; their technique is applied to τ in the present application. (Hereinafter we will usually refer to their paper as BK.) With calculations based on a theoretical model for coherent structures in wall turbulence, Landahl (1980) has found qualitative agreement with their conditionally sampled data.

The first question is whether $\tau(t)$ can be employed to obtain evidence about the bursting phenomenon and its stages. The idea comes from examination of the simultaneous measurements of $u(t)$ and $\partial u(t)/\partial y$ conducted by Eckelmann (1974). He showed that the fluctuating shear-stress signal from a wall shear-stress sensor correlates with velocity fluctuations measured with hot wires positioned in the flow at dimensionless distances from the wall of up to $y^+ = 25$. Eckelmann's correlation indicates that the temporal history of the shear-stress signal should provide a reasonable picture of turbulent events in the viscous layer, $0 < y^+ < 30$ in unaccelerated flows. In addition, Brown & Thomas (1977) have shown that the low-frequency fluctuations of a wall-shear sensor can be correlated with the low-frequency fluctuations of a velocity sensor for the range $0{\cdot}05 \leqslant y/\delta \leqslant 0{\cdot}75$ in a turbulent boundary layer. Eckelmann (1980 personal communication) notes that the detailed similarity between the two signals decreases with distance from the wall, so one must investigate whether one sees the same burst at $y^+ \approx 15$, the triggering location of BK, and at the wall. Some investigators expect that a conditionally averaged signal from a wall sensor will correspond to the conditionally averaged Reynolds shear stress (BK, figure 14). Thus a related question concerns the shape of the typical burst observed with a wall sensor, i.e. will our camel have one or two humps, or none?

A second question concerns the appropriate scaling of the bursting frequency f_b in non-accelerated flows. As discussed below, some investigators have suggested non-dimensionalization with respect to a characteristic time for the wall, or inner region, $\nu/(u_*)^2$; others advocate a time characteristic of the outer region, δ/U_∞. For a fully developed internal flow the two resulting non-dimensional times can be related through their definitions as

$$\frac{(u_*)^2}{\nu f_b} = \tfrac{1}{2}c_f Re_D \frac{V}{D_h f_b} = \begin{cases} \tfrac{1}{8}c_f Re_D \dfrac{2V}{s f_b} & \text{for ducts,} \\ \tfrac{1}{4}c_f Re_D \dfrac{V}{r_w f_b} & \text{for pipes,} \end{cases}$$

where Re_D is the Reynolds number based on hydraulic diameter D_h and bulk velocity V, and δ has been interpreted as $\frac{1}{2}s$, the half-spacing of a duct, or r_w, the radius of a pipe. Thus if a relationship can be found for one, it can be transformed to the other since empirical relationships for $c_f(Re_D)$ exist.

The question becomes one of whether either scaling will give a non-dimensional time or frequency which is independent of Reynolds number. The question of scaling is an important one for a better understanding of turbulent behaviour because inner scaling implies that the lift-up of the low-speed streak and the subsequent ejection

(Offen & Kline 1974) are derived from a wall-flow instability; theoretical models showing such instabilities have been proposed (Black 1968). (However, these instabilities cannot be unambiguously accepted as the causes of bursting because the instability models usually require (Black 1968) that the streamwise velocity of the ejected fluid be greater than the local mean velocity corresponding to the y^+ position of the ejection, rather than the velocity deficit actually observed.) Supporting evidence for inner scaling is offered by the flow-visualization data of Offen & Kline (1974), who found that sweeps, low-speed-streak lift-ups, and bursts were intimately connected; indeed, 'sweeps initiate bursts', and 'sweeps originate in the inner layer'.

Outer scaling implies that the bursting process is imposed by large disturbances already present in the outer flow. However, even Rao, Narasimha & Badri Narayanan (1971), early proponents of outer scaling, admitted that the 'origin of the bursting phenomenon cannot be traced directly...to the outer interface.' Outer scaling has its theoretical support too. The analysis by Schubert & Corcos (1967) attempted to view the inner layer as driven by the outer flow, but failed to predict Reynolds stresses of the right order. Brown & Thomas (1977) inferred from their measurements that the low-frequency fluctuations of the wall shear stress are possibly driven by large-scale structures.

Attempts to resolve the scaling issues experimentally have yielded mixed results. Black (1966) found that the bursting frequencies scaled with wall variables so that $(u_*)^2/\nu f_b \approx 110$. Kline *et al.* (1967) reported essentially the same finding for a boundary-layer flow, as did Corino & Brodkey (1969) for fully developed flow in a pipe. Sharma & Willmarth (1980) found the non-dimensional bursting frequency to be approximately constant over the range $1 \lesssim y^+ \lesssim 17$ when based on wall variables (this observation provides further support for the use of a wall-mounted sensor to investigate the bursting process as in the present work). In contrast, Rao *et al.* (1971) suggested that outer scaling resulted in Reynolds-number independence for unaccelerated flows, and that $U_\infty/\delta f_b = 5$ or $U_\infty/\delta^* f_b = 32$, where δ^* is the displacement thickness.

The results of Rao *et al.* must be regarded with some caution for two reasons. First, Blackwelder & Haritonidis (1981) found that sensor lengths greater than 20 viscous lengths yield decreased bursting frequencies as a consequence of spatial averaging. In a study conducted over a range of Reynolds numbers, the viscous length unit decreases with Reynolds number and the sensor becomes relatively larger. Blackwelder & Haritonidis suggest that the trends reported by Rao *et al.* are influenced by such effects, and that, when corrected for this spatial averaging, the results would support inner scaling.

Additionally, the finding of Rao *et al.* was based upon wind-tunnel measurements in which a single hot-wire signal was differentiated and a discrimination level varied to obtain a maximum f_b for each run. (It was stated that, as the discrimination level was set either too low or too high, f_b would decrease.) Offen & Kline (1974) indicate that such burst detection by a single sensor using autocorrelations has little chance of success, except very near the wall, because the individual bursts vary greatly in size. Thus detection techniques based upon spatial rather than temporal coherence are preferred. Flow-visualization studies, such as those by Kline *et al.* (1967) and Corino & Brodkey (1969), emphasize the more easily detected spatial coherence of bursts. A fixed point sensor can only measure the less organized temporal behaviour of the flow. Using the same apparatus as Kline *et al.*, Kim *et al.* (1971) determined bursting frequencies for two flows from visualization studies and from the disputed autocorrelation method with a hot wire at $y^+ = 14$. Because the Reynolds numbers

of the two flows were nearly equal, the results could be interpreted as supporting either inner or outer scaling.

Strickland & Simpson (1975) measured bursting frequencies in two ways: (i) the time between peaks in the autocorrelation of a wall-mounted shear-stress sensor was taken as a measure of the time between bursts, giving f_{b1}, and (ii) f_{b2} was taken to be the frequency at the maximum in the first moment of the curve of power-spectral-density versus frequency. They found agreement of the two frequencies to within 15%. While $U_\infty/\delta f_b$ ranged from 7 to 14, in fair agreement with Rao *et al.*, most of the flows examined were decelerating flows. For the two runs where the flow was mildly accelerated, $U_\infty/\delta f_b$ was approximately 11, twice the value recommended by Rao *et al.* The Reynolds numbers of the two flows were close enough ($Re_\theta = 2240$ and 3520) that, had a Reynolds-number dependence existed, it would not have been easily apparent. Indeed, in related work Strickland (1973) reported a weak Reynolds-number dependence.

Wallace, Brodkey & Eckelmann (1977) attempted to recognize bursts using a pattern-recognition technique based upon the time derivatives of hot-wire velocity sensors. They found that $U_\infty/\delta f_b$ ranged from 5 at $y^+ = 3$ to 2 at $y^+ = 300$. Although the agreement with Rao *et al.* was apparently good, only a single flow was investigated, so that Reynolds-number independence was not substantiated. Blackwelder & Kaplan (1976), using the variable-interval time-averaging (VITA) technique described below, also reported that $U_\infty/\delta f_b = 2{\cdot}8$, but, again, essentially only one Reynolds number was examined.

In summary, convincing evidence to support Reynolds-number independence for either method of scaling has yet to be published. In most studies investigators have not examined flows with a sufficient range of Reynolds number.† It might be supposed that this independence could be examined by simply combining studies (e.g. Wallace *et al.* (1977) at $Re_\theta = 430$ and BK at $Re_\theta = 2250$), but the dissimilarity of experimental methods, signal processing and detection criteria preclude an unambiguous comparison. Accordingly, one of our objectives was to measure a wide range of flows, both fully developed and accelerated, and to determine systematically if a preferred form of scaling became apparent.

We elected to use the VITA technique of BK, but, instead of employing this technique with hot-wire velocity sensors, we chose a wall sensor to avoid blockage and probe-interference effects, and, partly, to satisfy the objections raised by Offen & Kline (1974) regarding single-point sensors. As mentioned above, they pointed out that very near the wall the spatial variation of turbulent fluctuations is severely damped so that the temporal behaviour of a single sensor can become a reliable indicator of spatially coherent turbulent events. In other words, near the wall the temporal behaviour is not dominated by contributions from small-scale spatial variations, but reflects the passage of large-scale coherent structures; the wall film sensor is the ultimate in near-wall sensors. Furthermore, the VITA technique adopted was consistently applied to all 27 of the flows examined. Thus, even though the results may suffer from the usual uncertainty introduced by the subjective nature of pattern recognition schemes, at least the qualitative nature of the behaviour and trends reported should be correct.

In addition to determining the appropriate scaling of bursting frequencies for fully

† Preliminary results of the effects of wide ranges of Reynolds numbers and acceleration parameters have been presented informally by McEligot & Murphy (1978) for a converging duct and by Blackwelder & Haritonidis (1980) for a boundary layer; the present work extends the former and the manuscript by Blackwelder & Haritonidis (1981) extends the latter.

developed flows, we also wished to examine the effects of flow acceleration upon bursting. As noted in the review of Narasimha & Sreenivasan (1979) and in part 1, a variety of experimental techniques have been used to determine or to infer the flow regime of an accelerating flow: whether turbulent, laminar, laminarizing, laminarescent, etc. Further, definitions of the phenomenon called laminarization vary from author to author, depending on the technique used. The question arises whether the flow regime inferred by a comparison between a mean wall parameter and its prediction (e.g. part 1; McEligot 1963; Moretti & Kays 1965) would correspond to that determined from its transient signal of a pointwise sensor (Kline *et al.* 1967; Jones & Launder 1972). Thus the present paper investigates whether the indications of part 1 are consistent with temporal measurements of the bursting phenomenon in an accelerating flow induced by lateral convergence – at the same flow conditions in the same apparatus. This investigation then naturally leads to questions concerning the effects of acceleration on various aspects of the bursting phenomenon.

This paper is organized to respond sequentially to the questions introduced above. Section 2 presents the experimental procedures employed and demonstrates that a bursting signal can be identified from a wall sensor. The effects of Reynolds number on bursting in non-accelerated flows are examined in §3, and the results of acceleration due to lateral convergence are addressed in §4. Finally, the major conclusions are summarized in §5. An appendix treats some concerns related to the detection technique employed.

2. The experiment

The apparatus employed was the sector-shaped test section with pivoting siderails described in part 1; further details and tabulations of data are available (Murphy 1979; Chambers & Murphy 1981). For convenience, a number of pertinent parameters and results are summarized in table 1, which will be cited at various stages in the remainder of the paper.

2.1. *Ranges of variables*

Twenty-seven experimental runs were conducted over a range of conditions corresponding to part 1. Reynolds numbers based on bulk velocity V and hydraulic diameter D_h varied from 7600 to 47200 when evaluated at the location of the wall sensor, $x/s \approx 58$ (from the sharp-edged entrance). Since the cross-section had an aspect ratio of 12 or more, D_h was approximately equal to twice the plate spacing s. In the calculations of non-dimensional bursting periods $V/\delta f_b$ the boundary-layer thickness δ is evaluated as one-half the plate spacing; this approximation is considered later in the discussion of the results.

Convergent half-angles were set at 0°, 2°, 4°, 8° and 16°, resulting in a range of dimensionless acceleration parameters $K_V = (\nu/V^2)\,dV/dx$, from a nominal zero to $3{\cdot}4 \times 10^{-6}$. Based on the results of part 1 this variation would be expected to provide conditions from fully turbulent to near fully laminar flows at the sensor; examination of $dp(x)/dx$ in part 1 indicated that the apparent flow state – turbulent, laminar or intermediate – did not change significantly after $x/s = 20$. Bulk velocities varied from 6 to 40 m/s and mean wall shear stresses fell from 0·1 to 3·6 Pa.

2.2. *Surface sensor*

The surface shear-stress sensor and its calibration and operation are described in part 1. The heated filament of the sensor is 0·12 mm long in the flow direction and 1 mm

Run	Re_D	Convergence angle θ	$K_V \times 10^7$	Shear-sensor dimensions x^+	Shear-sensor dimensions z^+	Averaging time T (μs)	Record time length (s)	Low-pass filter cutoff frequency (kHz)	Digitization rate (thousands of samples/s)
1	47200	0	0	11·7	97·6	60	0·246	20	100
2	28500	0	0	8·16	68·0	120	0·492	20	50
3	23800	0	0	7·02	58·5	160	0·655	20	50
4	18800	0	0	5·76	48·0	240	0·983	20	50
5	13800	0	0	4·41	36·8	360	1·638	20	50
6	9100	0	0	2·64	22·0	1000	4·710	10	20
7	44500	2	2·08	11·8	98·4	60	0·246	20	100
8	26700	2	3·47	7·33	61·1	120	0·655	20	50
9	22200	2	4·18	6·19	51·6	200	0·901	20	50
10	17600	2	5·26	4·99	41·6	300	1·434	20	20
11	13000	2	7·11	3·80	31·7	500	2·253	20	20
12	8500	2	10·91	2·44	20·3	1200	5·734	10	10
13	42300	4	3·83	10·9	90·5	60	0·287	20	100
14	25500	4	6·36	7·00	58·4	160	0·655	20	50
15	21200	4	7·64	5·76	48·0	200	0·983	10	50
16	16900	4	9·61	4·76	39·7	320	1·475	10	50
17	12400	4	13·0	3·68	30·7	500	2·458	10	20
18	8100	4	20·0	2·23	18·6	1400	6·554	5	10
19	23800	8	10·9	6·49	54·0	160	0·819	10	50
20	19900	8	13·0	5·61	46·8	240	1·065	10	50
21	15700	8	16·5	4·45	37·1	360	1·638	5	50
22	11700	8	22·0	3·12	26·0	800	3·482	5	20
23†	7600	8	33·9	1·88	15·7	2000	9·011	0·5	5
24	21900	16	16·9	5·67	47·3	240	1·065	10	50
25	18300	16	20·3	4·92	41·0	300	1·434	10	20
26	14700	16	25·3	3·94	32·9	500	2·253	5	20
27	11000	16	33·9	2·71	22·6	1000	4·506	2	10

Run	No. of bursts	Bursting frequency f_b (Hz)	$\frac{2V}{f_b s}$	$\frac{(u_*)^2}{\nu f_b}$	Ratio of sweep time to time between bursts	$c_f = \frac{2\bar{\tau}}{\rho V^2}(\times 10^2)$	$\frac{\tau_{rms}}{\bar{\tau}}$
1	315	1282	4·88	150	0·121	4·80	0·0567
2	287	584	6·52	160	0·108	6·36	0·0586
3	225	343	9·22	202	0·075	6·77	0·0590
4	235	239	10·47	195	0·072	7·31	0·0594
5	181	110	16·7	248	0·055	7·90	0·0601
6	305	64·8	18·7	151	0·072	6·59	0·0648
7	225	916	6·47	216	0·084	5·61	0·0514
8	185	282	12·6	270	0·055	6·00	0·0584
9	215	239	12·3	228	0·060	6·20	0·0577
10	278	208	11·3	170	0·099	6·40	0·0573
11	213	94·5	18·4	217	0·056	6·78	0·0594
12	242	42·2	26·8	200	0·063	6·57	0·0612
13	190	663	8·40	253	0·072	5·36	0·0514
14	172	262	12·8	265	0·064	6·11	0·0575
15	150	153	18·4	309	0·029	6·00	0·0579
16	147	100	22·3	323	0·045	6·48	0·0584
17	125	50·9	32·2	379	0·040	7·14	0·0551
18	115	17·5	61·0	404	0·045	6·15	0·0546
19	100	122	25·4	489	0·039	6·20	0·0566
20	107	100	25·8	446	0·036	6·63	0·0551
21	84	51·3	40·0	550	0·031	6·66	0·0559
22	66	19·0	81·0	729	0·038	5·85	0·0486
23†	13	1·44	690	3495	0·010	5·07	0·0286
24	127	119	23·7	383	0·047	5·71	0·0572
25	107	74·6	31·5	460	0·039	6·18	0·0538
26	55	24·4	77·5	906	0·024	6·17	0·0524
27	29	6·44	219	1623	0·021	5·23	0·0352

† AC coupled to signal conditioner at 2 Hz. All other cases a.c. coupled at 0·1 Hz.

TABLE 1. Signal-processing parameters and principal results

wide in the spanwise direction; it was located at $x/s = 58$ on the duct centreline. The sensor and its support were flush with the surface to within 15 μm, which in the worst case (high Reynolds number) corresponded to a height of 1·5 viscous units, well within the viscous sublayer.

2.3. *Signal processing and burst detection*

The sensor mean voltage was measured with an integrating digital voltmeter, and the fluctuating component was recorded at 60 in./s on an f.m. tape recorder. Before recording, the fluctuating signal was filtered and amplified. The high-pass cutoff frequency was 0·1 Hz, 60 times smaller than the minimum bursting frequency determined in the experiments as shown in table 1. The low-pass cutoff frequency ranged from 500 to 20000 Hz, depending upon Reynolds number and acceleration; it was at least 16 times the bursting frequency, and, more typically, about 100 times the bursting frequency. The taped signals were analysed at digitization rates of 5×10^3–10^5 samples per second, as shown in table 1. A BASIC program was written to read the digitized sensor-voltage fluctuations, to add the separately measured d.c. sensor voltage, and to calculate the instantaneous wall shear stress using the calibration relation. Additional details are presented by Chambers & Murphy (1981).

The conditioned signal analysis was performed using the VITA technique described by Blackwelder & Kaplan (1976). The validity of this technique was examined in their original paper; they concluded that the conditionally averaged results are closely related to the turbulence structure and not to the detection criteria. For further details the reader is referred to their paper.

The variance of the wall shear stress was defined as

$$\text{var}\,(t, T) = \hat{\tau}^2(t, T) - [\hat{\tau}(t, T)]^2, \tag{1}$$

where $\hat{\tau}^2(t, T)$ is the running average of the square of the wall shear-stress signal over the conditional averaging period T:

$$\hat{\tau}^2(t, T) = \frac{1}{T}\int_{t-\frac{1}{2}T}^{t+\frac{1}{2}T} \tau^2(t)\, dt, \tag{2}$$

$$\hat{\tau}(t, T) = \frac{1}{T}\int_{t-\frac{1}{2}T}^{t+\frac{1}{2}T} \tau(t)\, dt. \tag{3}$$

When T becomes very large, conventional averaging is obtained. The variance of the shear stress, (1), represents a localized measure of the amplitude of a turbulent shear-stress fluctuation.

In their original proposal, designed for hot-wire velocity sensors immersed in the flow, Blackwelder & Kaplan suggested that, since bursting is an energetic process, an *ad hoc* detection criteria could be defined as

$$D(t) = \begin{cases} 1 & \text{if var} > k\tau_{\text{rms}}^2, \\ 0 & \text{otherwise}, \end{cases} \tag{4}$$

where k is the threshold level selected. The quantity τ_{rms} is the root mean square of the fluctuating shear stress obtained by integration over a long time,

$$\tau_{\text{rms}}^2 = \lim_{T \to \infty} (\text{var}), \tag{5}$$

which is independent of time because of stationarity. BK used a value of 1·2 as k for their velocity measurements at $y^+ = 15$.

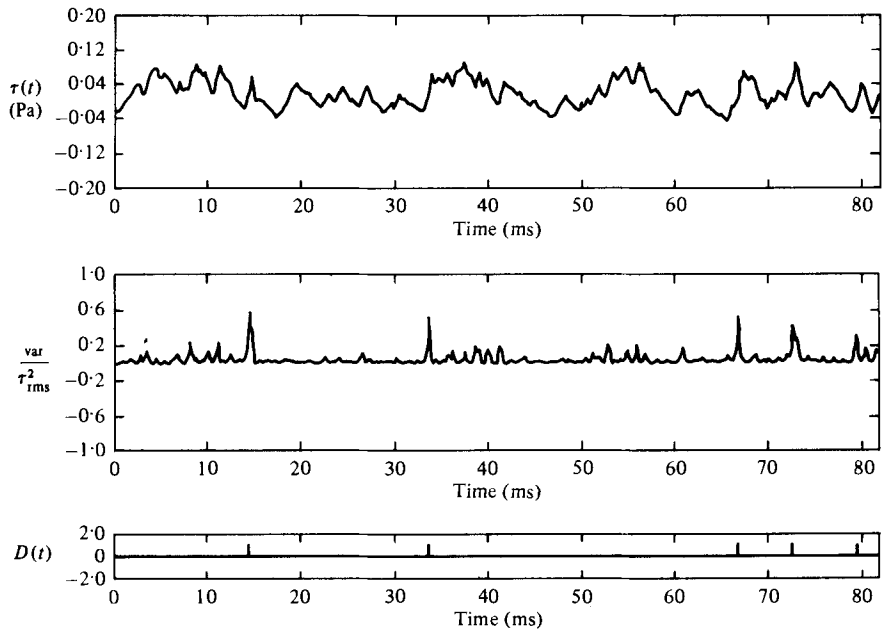

FIGURE 1. Typical wall shear-stress signal and detection parameters: $Re_D = 15700$ and $K_V = 1{\cdot}6 \times 10^{-6}$.

BK also recommended that the time period T for the short-term averages be calculated from the relation

$$T^+ = Tu_*^2/\nu = 10. \tag{6}$$

As noted earlier, Eckelmann (1974) showed that fluctuations of wall shear stress and velocity are well correlated in the wall region. The ejections, sweeps and other phenomena that characterize bursts also appear in this region, and hence the correlation suggests that the bursting frequencies determined by either a wall sensor or a velocity sensor in this region would be nearly the same. Thus the recommendation of BK regarding the averaging time, (6), was followed with the minor exception that restrictions upon digitization rates available resulted in differences of $\pm 5\,\%$ from the recommended values of T. The total record lengths of the signals examined ranged from $4500T$ to $5100T$, which was usually adequate. Record lengths and averaging times employed are shown in table 1.

Next the threshold level k must be considered. Turbulent velocity fluctuations are damped as the wall is approached. However, this damping is no more rapid than the diminishment of y itself, so that the fluctuation of wall shear stress, i.e. the gradient of the velocity fluctuation at $y = 0$, is of finite value. Nevertheless, it would be fortuitous if the required value of k turned out to be the same for the wall signal as BK determined for velocity at $y^+ = 15$.

A typical segment of a sample record for the shear-stress fluctuation about the mean,† $\tau(t)$, calculated from the filtered and digitized anemometer voltage via the calibration relation, is presented in figure 1 (*a*). The corresponding values of the short-term variance, non-dimensionalized by the r.m.s. shear stress $\mathrm{var}/\tau_{\mathrm{rms}}^2$ and the detector function $D(t)$, are presented in figures 1 (*b*) and (*c*) respectively, for $k = 0{\cdot}3$

† In part 1, τ referred unambiguously to the mean wall shear stress. In the present paper the mean is represented by $\bar{\tau}$ while τ is the fluctuation.

as the threshold level. It may be observed in figure 1 (*b*) that the non-dimensionalized variance becomes large when the shear-stress fluctuation exhibits rapid increases (large positive slope). Figure 1 (*c*) reveals that with $k = 0{\cdot}3$ five events believed to be associated with the bursting process (it will later be argued that the events are sweeps) are detected in this record segment. Further observation indicates that the detected events are characterized by sudden large increases in τ, generally followed by somewhat slower decreases. If one examines the signal directly above the detected events, one may discern extremely steep slopes – or rapid accelerations – relative to the other fluctuations.

The subjective nature of the choice of k is apparent in the figure. A lower value of k would yield a larger number of detected events, while a higher value would yield a lesser number. For reasons discussed in the appendix, we found it appropriate to reduce the value of k from 1·2 to 0·3. This required increase in detection sensitivity is believed attributable to two causes: (i) the lower magnitude of wall shear-stress fluctuations compared with fluctuations in velocity at $y^+ = 15$, and (ii) the possibility that the large dimensions of the heated filament may have resulted in further reduction of the sensitivity to bursts as discussed below. Due to the wide variation of Reynolds number and acceleration both Δx^+ and Δz^+ of the sensor filament vary widely, from 2 to 12 and 16 to 98 respectively.

Kline *et al.* (1967) and Willmarth & Lu (1971) suggested that the spanwise separation between the streaks of low-speed fluid that appear in the early stages of bursting is $\Delta z^+ \approx 100$. Simpson (1976) measured short-time correlations between wall sensors with variable spacing Δz^+ and found high values for $\Delta z^+ \approx 10$, zero for $\Delta z^+ \approx 30$ and maximum negative values with $\Delta z^+ \approx 50$. Likewise, Blackwelder & Eckelmann (1978) showed that the correlation of the streamwise wall shear-stress fluctuations was 0·5 when the two sensors were separated by the distance $\Delta z^+ = 25$, and the zero-crossing occurred at $\Delta z^+ = 35$. Consequently it would be expected that the sensitivity of the sensor used in this work would be muted – for example, the wider the non-dimensional size, the more negative fluctuations could contribute to the signal at the same time as a positive fluctuation (see Simpson's figure 8), so that the total signal is smaller than the positive fluctuation. This diminished sensitivity provides one reason for the necessity for using a low level of threshold triggering in the conditional sampling.

As Δz^+ increases one expects an increase in the rate of burst interception, but a decrease in their apparent magnitudes due to the spatial averaging. With the detection threshold kept constant, it is not clear whether the rate of detected bursts should increase or decrease as Δz^+ increases. Since the measured value of τ_{rms} is subject to the same effects, it is believed that normalizing the signal as $\mathrm{var}/\tau_{\mathrm{rms}}^2$ should compensate for the size effects to some extent. However, by experimenting with hot-wire sensors of varying lengths l^+ at $y^+ \approx 15$ while applying the same detection scheme, Blackwelder & Haritonidis (1981) found measured bursting frequencies to decrease when $l^+ \lesssim 20$. There is currently no evidence as to whether this trend would be present for wall sensors as well as immersed hot wires. The possible effects of non-dimensional size on the present results are also considered later when they are presented.

In the appendix, the effects of varying the threshold k are investigated. It is shown that our conclusions are rather insensitive to the choice even if k is either halved or increased by one-half.

An additional detection criterion employed was to require that the shear stress be increasing at the beginning of an event. The occurrence of ejections would result in

decreases in the shear stress, whereas a sweep, an inward motion of fluid with increased streamwise velocity, would result in an increase in shear stress. Therefore this additional criterion has the effect that each burst is detected in its sweeping phase.

Offen & Kline (1974) found, with dye and hydrogen-bubble visualization methods, that 83 % of the sweeps they identified were traced to ejections – the unaccounted 17 % were felt to be due to inadequacies in the methods they used. It appears then that there is little or no difference in determining burst events by either counting ejections or sweeps, and in the remainder of this paper the sweep frequencies reported will be referred to as burst frequencies. However, other quantities to be defined later will appropriately be referred to in terms of sweep quantities, e.g. 'sweep times'.

The requirement that the shear stress be increasing was implemented with a simple test of whether the shear stress at a point meeting the detection criterion (4) was greater than that at five points before it, following a similar technique employed by Blackwelder (1978). The choice of five points was arbitrary, but was felt to be stringent enough to separate sweeps from other events. It was found that, when τ was decreasing, very few points met the threshold criterion, indicating that the sweeps are the more energetic component of the bursting process at the wall. Thus the arbitrary choice of five points for the slope test was of little significance.

2.4. *The typical burst/sweep event and definition of related quantities*

The beginning of the detection of a sweep was defined as the point at which the two detection criteria were first satisfied. The next point at which the threshold criterion was not met was considered to be the end of the sweep detection. The number of sweeps and the time duration of the individual sweep detections were determined in the numerical program. The burst frequency was defined as the number of sweeps detected divided by the total time of the record.

The number of sweeps detected ranged from 13 to 315, with most records having more than 65. The average number detected was 167. Burst frequencies varied from 1·4 to 1280 Hz. Other details of the signal processing and some of the averaged results are listed in table 1.

An ensemble average was formed from the time history of the shear stress preceding and following the time of initial detection of each sweep. This conditional average of the shear-stress signal $\langle \tau(t) \rangle$ then could be considered to be a representation of the typical burst/sweep phenomenon for the run. As shown later, the typical pattern of these averages shows a very sharp increase in shear stress followed by a more gradual decline after the peak value is attained. Preceding the sweep is a general reduction of τ, and following it is evidence of generally quiescent behaviour. The general features observed are similar to the conditional averages of streamwise velocity fluctuations measured by BK at $y^+ = 15$, but some details differ.

In the present study all the conditional averages of $\tau(t)$ exhibit the same general shape. This observation provides some confidence that meaningful information can be deduced by applying the burst-detection scheme described above.

In order to quantify the shape of the conditional averages, sweep times and magnitudes are defined. The magnitude $\Delta\tau$ is taken as the difference between the peak value and the minimum immediately preceding detection. With a wall sensor or a single wire the time elapsed during a sweep towards the wall cannot be determined as well as with an X-probe. For the present purposes a sweep time is defined which is a relative measure of the width of the averaged burst signal; it is taken as the time from when the signal rises to $1-e^{-1}$ of its maximum value until it falls through this level when decreasing (this definition is considered to be an improvement over the

one used by Chambers & Murphy (1981)). Since the rise is quite sharp, this time interval is primarily a time constant for the decay of the conditioned sweep.

3. Effects of Reynolds number

With the convergence angle set at zero the test section forms a rectangular duct with a constant cross-section. Measurements in part 1 showed that in this configuration the pressure gradient becomes essentially constant after $x/s \approx 20$, so the wall sensor at $x/s \approx 58$ determines the shear stress for an approximately fully developed flow.

The data covered the range $9100 \leqslant Re_D \leqslant 47200$ in this series. Pressure-drop measurements, used to calibrate the shear-stress sensor, agreed with the Blasius relationship $c_f = 2\tau/\rho V^2 = 0{\cdot}0791\, Re_d^{-\frac{1}{4}}$, within an average of about 6% with a maximum deviation of less than 8%.

3.1. *Bursting frequencies*

The bursting frequencies f_b determined with the VITA technique are presented in table 1. For these fully developed runs f_b ranged from 65 to 1280 Hz; the dimensionless bursting periods (reciprocal frequencies) based upon inner scaling, $(u_*)^2/\nu f_b$, were approximately constant at 180, while the outer scaled period $V/\delta f_b$ or $2V/sf_b$ ranged from 5 to 19. The value of $(u_*)^2/\nu f_b$ found here is 60% higher than that of Black (1966); the values of $V/\delta f_b$ are 1–4 times that of Rao *et al.* (1971) and nearly the same as the range given by Strickland & Simpson (1975). Considering the wide disparity of the detection techniques used, choices of threshold criteria and the subjectiveness that is an inescapable component of all the techniques, we regard the agreement of all these results, taken collectively, as surprisingly good.

More important than the absolute values of either $(u_*)^2/\nu f_b$ or $V/\delta f_b$ are the variations of these quantities with Reynolds number; these trends are displayed in figure 2. Also plotted for convenience is the dimensionless quantity $V^2/\nu f_b$ (Rao *et al.* 1971); in nearly every flow V and ν are known or easily estimated, but u_* and δ often require additional calculation or separate measurement. Thus f_b could be estimated directly if a useful relationship for $V^2/\nu f_b$ were available. Alternative versions of mixed scaling, such as $u_* V/\nu f_b$, lack this advantage.

There is more scatter than one would desire in each of the plots of figure 2 but, as mentioned earlier, $(u_*)^2/\nu f_b$ is nearly constant, whereas $2V/sf_b$ and $V^2/\nu f_b$ exhibit Reynolds-number dependence. The straight lines drawn through the data are the values one would expect if $(u_*)^2/\nu f_b$ is independent of Re_D and equal to 180. The relationship for $2V/sf_b$ is based on the Blasius relation for skin-friction coefficient and the definition, as explained in §1, and the one for $V^2/\nu f_b$ is a direct extension (Chambers & Murphy 1981).

The agreement between the data and the trends of these relationships, $(u_*)^2/\nu f_b \approx$ constant and $2V/sf_b \propto Re^{-\frac{3}{4}}$, provides support to the thesis that scaling bursting frequencies with inner variables is the more useful approach for fully developed flow. In unpublished work during the writing of this manuscript, Blackwelder (1980, personal communication), Sharma & Willmarth (1980) and Sreenivasan (1981 personal communication and Sreenivasan, Prabhu & Narasimha 1982) have reported comparable conclusions for turbulent boundary layers.

If it were possible to account for the variation of wall sensor size, Δx^+ by Δz^+, in the present study, it is likely the relationships would be affected, but the conclusion that inner scaling is preferable would not. Examination of the data of Blackwelder & Haritonidis (1981) for the effects of hot-wire length on bursting measurements

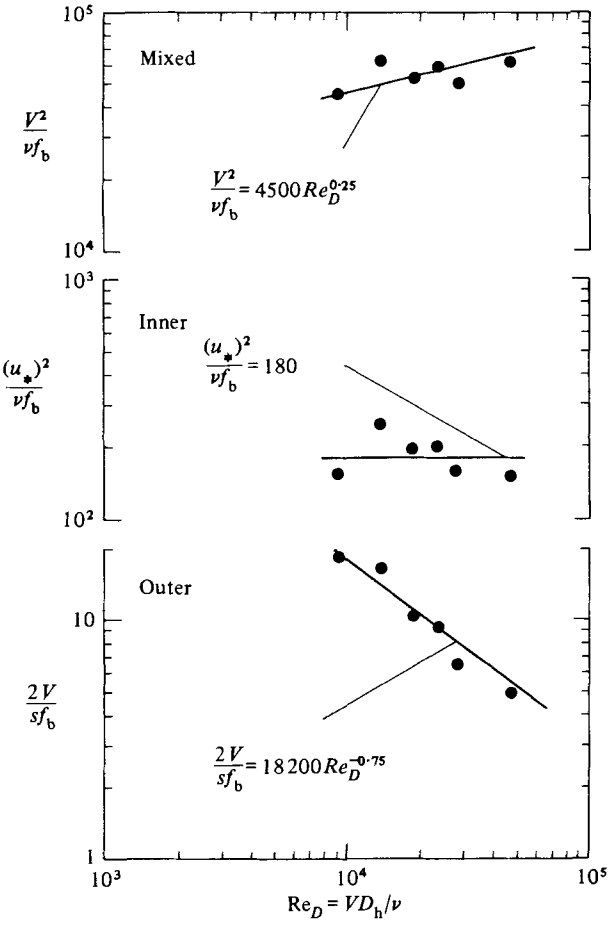

FIGURE 2. Average bursting periods for fully developed flows.

suggests that – if the effects on wall shear-stress sensors are similar – the bursting frequencies presented for our highest Reynolds numbers are too low. For inner scaling a burst-period curve corrected with their relationship would slope downward; it would not be constant. It would still, however, exhibit smaller variation than a curve for outer scaling with the same relation applied.

3.2. *Conditionally averaged sweep patterns*

Conditionally averaged sweep patterns for the six fully developed flows are shown in figure 3, and it may be noted that the shapes are generally the same. As noted earlier, there are some slight differences from the conditional averages of streamwise velocity fluctuation measured by BK at $y^+ = 15$. Their conditional averages appear more antisymmetric about the detection time (see their figure 10) than the present pattern of $\tau(t)$. In particular, in the present work the minimum just preceding the sharp increase in τ, is less severe and less abrupt; this observation might be interpreted partly as indicating that at the wall the timing of the effects of an ejection phase are less well correlated with the effects of the sweep than at $y^+ = 15$.

Blackwelder (1980 personal communication) reports that in the near-wall region the sweeps are the predominant events. He finds that at $y^+ \approx 15$ the effects of ejections and sweeps are equally felt. Above $y^+ = 15$ the most important aberrations

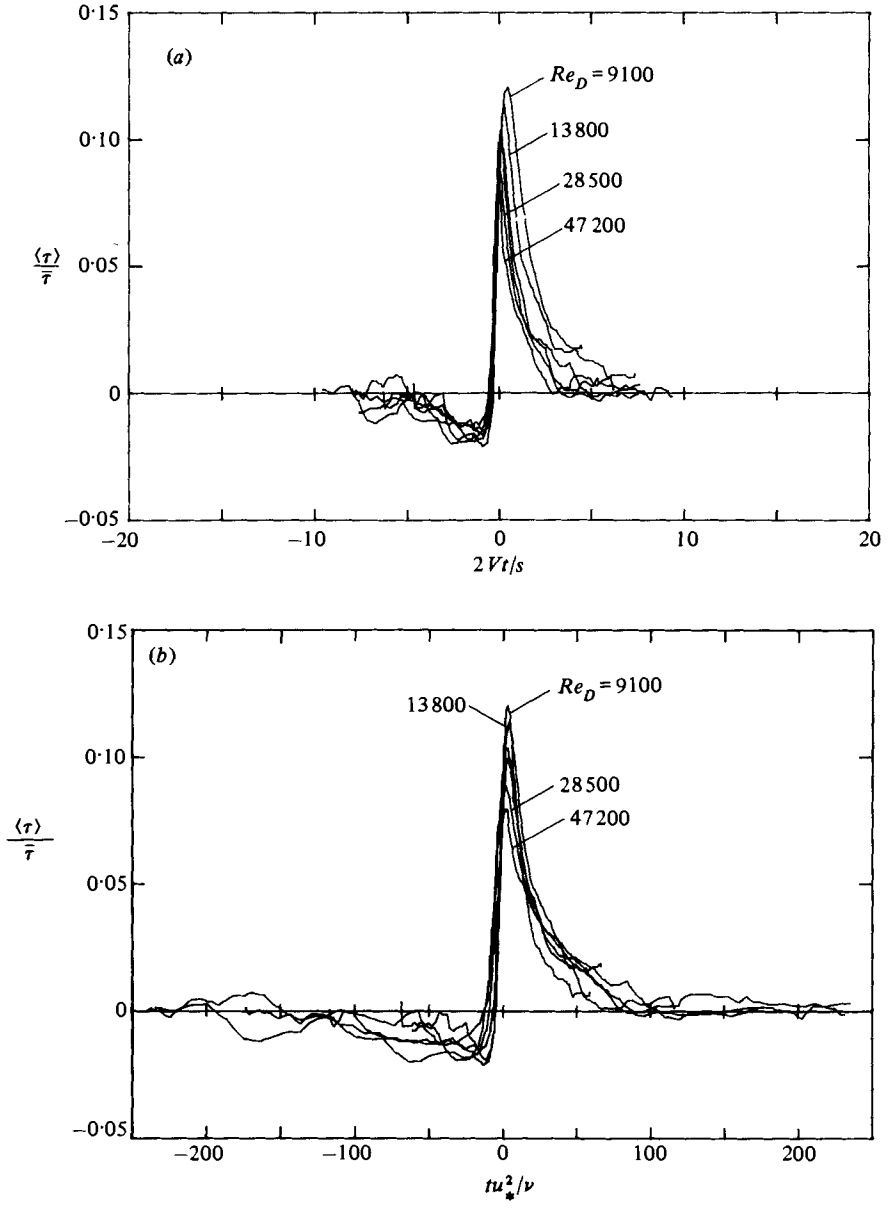

FIGURE 3. Conditionally averaged wall shear-stress fluctuation for fully developed flow: (*a*) outer variables; (*b*) inner variables.

in the flow field are due to ejections leaving the wall. Below $y^+ = 15$ the strongest changes in the streamwise velocity are primarily due to sweeps buffeting the wall area. This is evident in the earlier conditional averages of BK and can be seen in the probability-density distributions of Eckelmann (1974). Thus, at the wall, one does not see a significant decelerating low-speed region before the short acceleration.

Blackwelder reports unpublished conditional averages of the wall shear stress in Reichardt's oil channel; the shapes were very similar to the present ones. Likewise, Zakkay, Barra & Hozumi (1979) present conditionally averaged values of wall shear stresses similar to those in figure 3 obtained by using both velocity and wall shear-stress

signals for detection. A. S. W. Thomas (1981 personal communication) also has mentioned finding patterns resembling ours.

Since Eckelmann (1974) reports that the correlation coefficient between $u(y)$ and $(\partial u/\partial y)_0$ drops to about 50 % near $y^+ = 15$, it is not surprising that the velocity and shear-stress burst patterns differ somewhat. However, the present burst pattern definitely does not resemble the double-peaked pattern of the conditional averages of Reynolds shear stress as determined by BK.

For examination of effects of varying the Reynolds number, the data for the six fully developed flows have been superimposed in figure 3 with time axes scaled again with outer and inner variables. There are slight, approximately systematic, variations in both cases. The magnitude $\Delta\tau/\bar{\tau}$ tends to decrease with increasing Reynolds number; there is a change of about 50 % over the range from $Re = 9100$ to 47200. Normalized by $\tau_{\rm rms}$ the non-dimensional magnitude $\Delta\tau/\tau_{\rm rms}$ decreases slightly less over the same range. The variation of width (or sweep time) is discussed below. The use of inner variables for the non-dimensional time appears to provide slightly better scaling.

The weak Reynolds-number dependence of these results may in part be a consequence of the fixed size of the shear-stress sensor element. As noted in the discussion of burst detection, since the sensor is of fixed physical size, its non-dimensional size, Δx^+ by Δz^+, increases with Reynolds number. Whether this variation affects the shapes of the conditionally averaged patterns discussed here is a question that is considered to be an appropriate topic for later experiments or modelling.

3.3. *Sweep time*

The sweep time $t_{\rm s}$ as defined in §2.4 is a measure of the average duration during which the sweep phase of the burst is most energetic or, presumably, has its highest velocity. It should not be confused with the mean time between sweeps or average bursting period, i.e. the inverse of $f_{\rm b}$. As with $f_{\rm b}$, $t_{\rm s}$ was scaled with inner, outer and mixed variables; the behaviour for the fully developed flows is presented in figure 4.

With any of the three bases for scaling time, the non-dimensional sweep time varies with Reynolds number, as is evident from viewing the shapes in figure 3 as well. As with the bursting frequency, inner scaling provides the least sensitivity to Reynolds number of the three.

If one approximates the sweep time in inner variables to increase as $Re^{\frac{1}{4}}$, as seen earlier in figure 4, relationships analogous to the non-dimensional relation for $f_{\rm b}$ can again be derived for outer and mixed scaling of $t_{\rm s}$ via the definitions and the Blasius friction relation. These predicted trends are shown as solid lines on figure 4 and agree well with the data.

The product of the sweep time and the bursting frequency $t_{\rm s} f_{\rm b}$ is the ratio of average sweep time to average period between bursts (or sweeps) and is therefore called the sweep-time ratio. It represents the average fraction of time between bursts or fraction of total time that the most energetic part of the sweep process occurs (as defined in §2.4; it is listed in table 1). An alternative view is that it is like an intermittency function for the most energetic part of the bursting process, but its maximum is not necessarily unity. By considering the results in terms of inner variables in figures 2 and 4, one can see that this fractional time or intermittency gradually increases from about 6 to 12 % with some scatter as the Reynolds number is increased from 9100 to 47200 (on semilogarithmic co-ordinates).

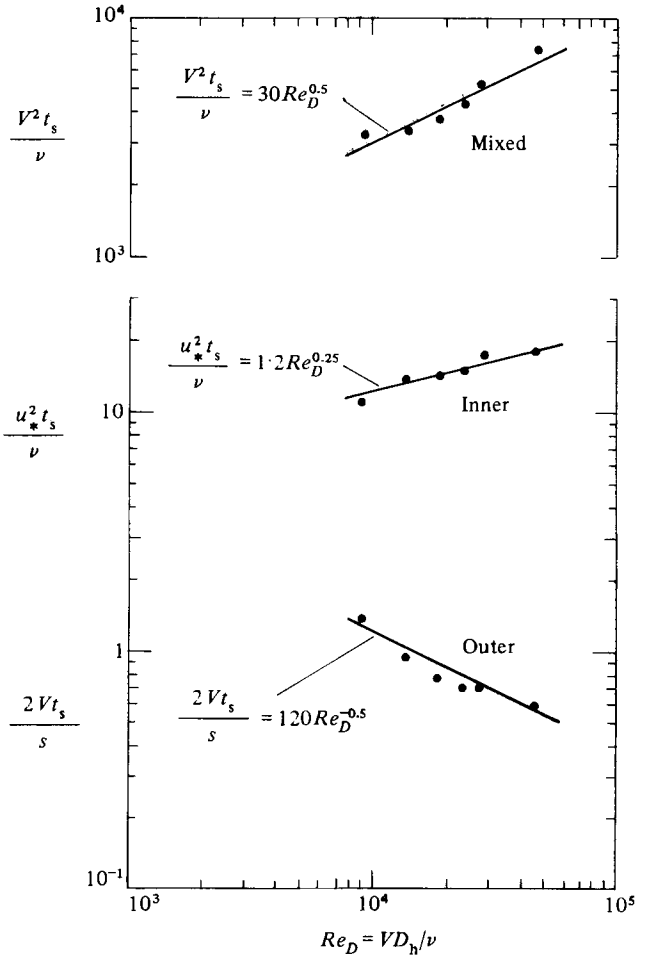

FIGURE 4. Dimensionless sweep times for fully developed flow.

4. Laterally converging flow

In part 1 it was shown that streamwise pressure distributions and mean wall shear stresses measured in laterally converging flow agreed with numerical predictions based on a van Driest turbulence model provided that the acceleration parameter K_V was less than about 10^{-7}. Above $K_V \approx 4 \times 10^{-6}$ the data corresponded to laminar predictions. For the intermediate range between these values, agreement could be obtained by empirically adjusting the parameter A^+ which controls the effective viscous-layer thickness predicted by the model.

By flow visualization with hydrogen bubbles and dye streaks in turbulent flow between two converging flat plates, Kline *et al.* (1967) determined that a non-dimensional breakup (ejection) frequency in the viscous layer decreased as the acceleration parameter K_V increased. They also attempted to determine the dependence of streak spacing from $K_V \approx -2 \times 10^{-6}$ to $K_V \approx 1 \times 10^{-6}$, but their plotted results appear inconclusive.

In addition to examining the effect of acceleration on the bursting rate, we wished to determine the behaviour of other characteristics of the bursting process and to investigate the correspondence to the integral measurements of part 1. Accordingly,

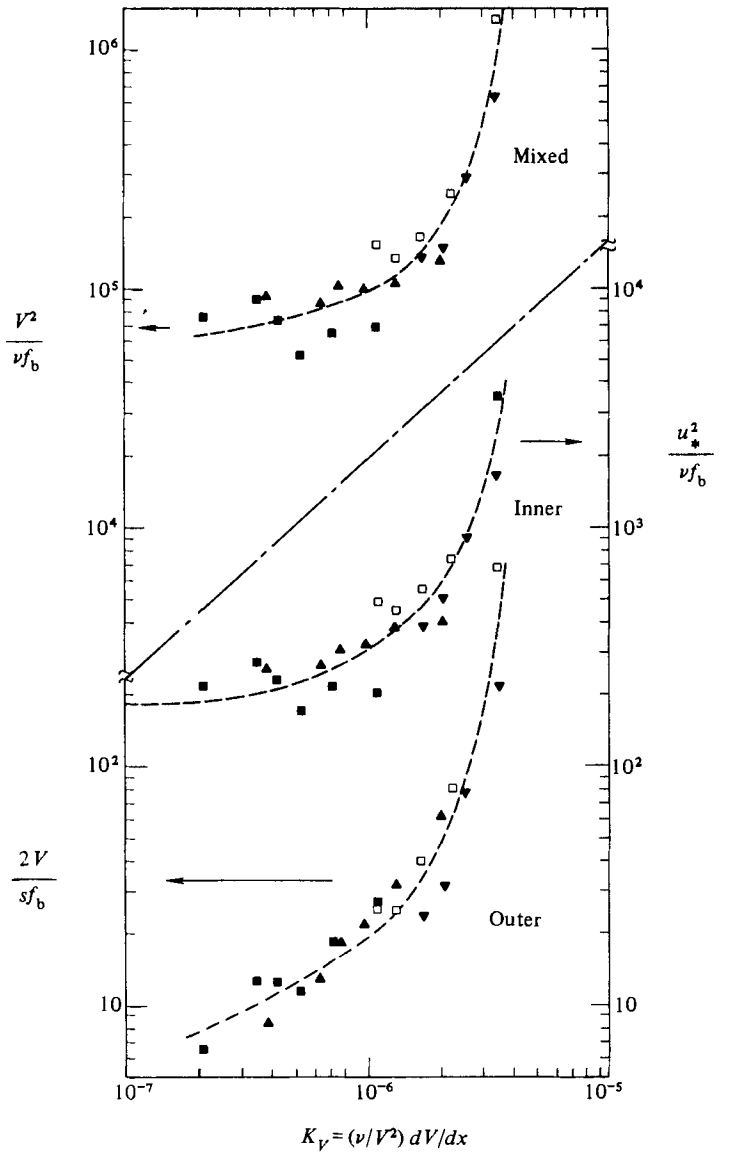

FIGURE 5. Average bursting periods (inverse of bursting frequency) for laterally converging flows: ■, $\theta = 2°$; ▲, 4°; □, 8°; ▼, 16°; ----, best fit.

the test section was operated with the siderails at θ from 2° to 16° to cover approximately the same range of flow conditions as in part 1.

4.1. *Bursting frequencies*

The effects of acceleration upon bursting frequencies are apparent in figure 5. No matter how they are scaled, all the dimensionless frequencies suggest a significant decrease in f_b or increase in its inverse, the average period, as K_V increases.

Focusing upon the inner scaling of f_b, shown earlier to be the most appropriate scaling in the case of fully developed flows, one finds that as K_V decreases towards 10^{-7} the bursting frequency approaches the values observed for fully developed turbulent flows. At $K_V = 1 \times 10^{-6}$, $u_*^2/\nu f_b$ is 300, nearly 70 % higher than the value

at $K_V = 0$; at $K_V = 2 \times 10^{-6}$ one finds a threefold increase, and $K_V = 3{\cdot}4 \times 10^{-6}$ indicates a fifteenfold increase, with the curve beginning to tend asymptotically towards infinity. This tendency implies that the flow would be effectively laminar for K_V larger than about $3{\cdot}4 \times 10^{-6}$. This finding is in accord with the data of part 1 in the same test section and with the data of Moretti & Kays (1965), Kline *et al.* 1967), Blackwelder & Kovasznay (1972) and Jones & Launder (1972) in different geometries using other techniques. The agreement on the value of K_V for apparent laminarization assures one that the earlier studies, based upon flows in nozzles or between inclined plates in which the contraction was due to reduction in the direction perpendicular to the plates rather than in the lateral (spanwise) direction as in the present study, are valuable guides to prediction of laminarization regardless of geometry. As in part 1, the value of K_V where the results begin to differ significantly from the fully turbulent case is less clear, but using the best-fit curve as a guide it might be taken as near $K_V = 6 \times 10^{-7}$.

The same asymptotic increase in burst period as K_V increases near $3{\cdot}4 \times 10^{-6}$ is evident when the results are presented in terms of outer scaling $2V/sf_b$. The use of $\frac{1}{2}s$, the half-plate spacing, instead of δ, the boundary-layer thickness, only makes the trend more conservative, since any boundary-layer thinning with acceleration would accentuate the increase in outer scaled burst period with acceleration parameter. If one applies the results of Blackwelder & Haritonidis (1981) for hot-wire probes, correction for spatial averaging effects in the wall shear-stress sensor would also tend to accentuate this trend. (Exaggerating this effect further is the observation by Simpson (1979) that the spacing λ_z^+ of the streamwise structures increases as the acceleration parameter increases.) These corrections would tend to increase burst frequencies at the high Reynolds numbers which correspond to the lower values of the acceleration parameter. Thus, burst periods would be decreased further at the left side of the curve. We also note that as K_V decreases there is no obvious approach to the corresponding fully developed, turbulent behaviour since $2V/sf_b$ varies with Re_D in that case. To provide a meaningful criterion for a fully turbulent limit on the basis of $2V/sf_b$ would require consideration of K_V and Re_D simultaneously.

4.2. *Conditionally averaged sweep patterns*

Families of conditionally averaged time histories have been selected at approximately equal Reynolds numbers and varying acceleration parameters to compare with the results for fully developed flows. Figure 6 presents typical results versus both outer and inner time scaling at a Reynolds number of about 12000. Additional families were compared at $Re \approx 8000$, 18000 and 23000 with the same qualitative conclusions.

At a given Reynolds number, neither time scaling shows a clear advantage over the other. Also, there is no large variation in the shape of the time-averaged signals until the acceleration parameter reaches $K_V \approx 2 \times 10^{-6}$. That is, the sweep pattern is essentially invariant until K_V approaches this value even though the non-dimensional bursting frequency begins to drop considerably for $K_V \gtrsim 1 \times 10^{-6}$. At higher values than $K_V \approx 2 \times 10^{-6}$ the recovery or decay of the sweep phase becomes slower than in the fully developed or moderately converging runs in either time scaling.

Considering the magnitude of the peak of the event, defined previously as $\Delta\tau$, one may observe different behaviour when non-dimensionalized by $\bar{\tau}$ and by $\tau_{\rm rms}$. There is some scatter in the non-dimensional magnitudes $\Delta\tau/\bar{\tau}$ but no clear trend versus K_V. When normalized as $\Delta\tau/\tau_{\rm rms}$ there is evidence of an increase in magnitude as K_V increases above 10^{-6}. As may be seen in table 1, this latter observation is partially

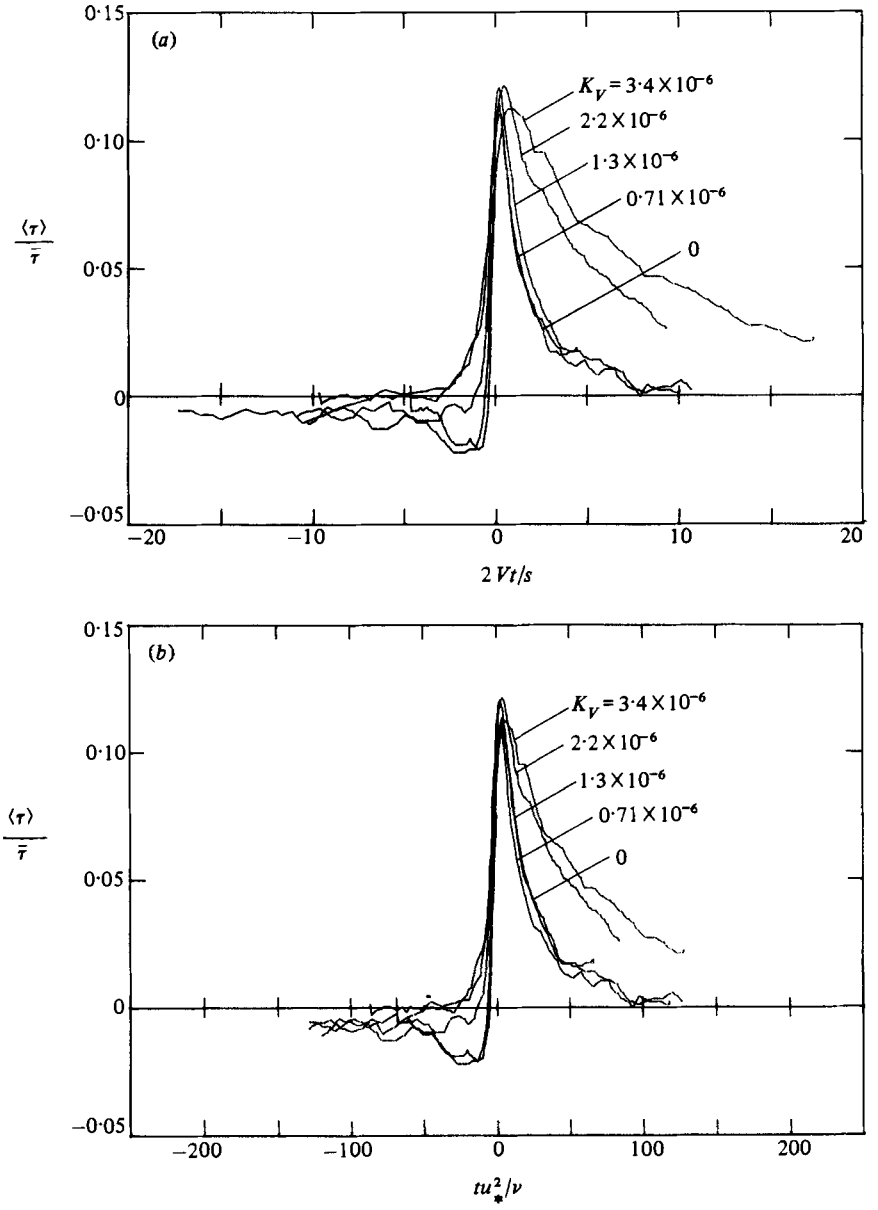

FIGURE 6. Conditionally-averaged wall shear-stress fluctuation in laterally converging flow; $11000 \lesssim Re_D \lesssim 13800$, $0 \lesssim K_V \lesssim 10^{-6}$: (*a*) outer variables; (*b*) inner variables.

a consequence of a decrease in $\tau_{\rm rms}/\bar{\tau}$ in some runs at large acceleration parameters. The burst events may consequently be considered to provide a greater percentage of the total turbulent activity in the cases of higher acceleration.

4.3. *Sweep times*

The widths of the conditionally averaged traces can be studied in terms of the characteristic time defined in §2.4 and called the sweep time in the present work. These times are presented in figure 7 in terms of inner, outer and mixed scaling with the lateral convergence angle θ (which causes the acceleration) used as a parameter.

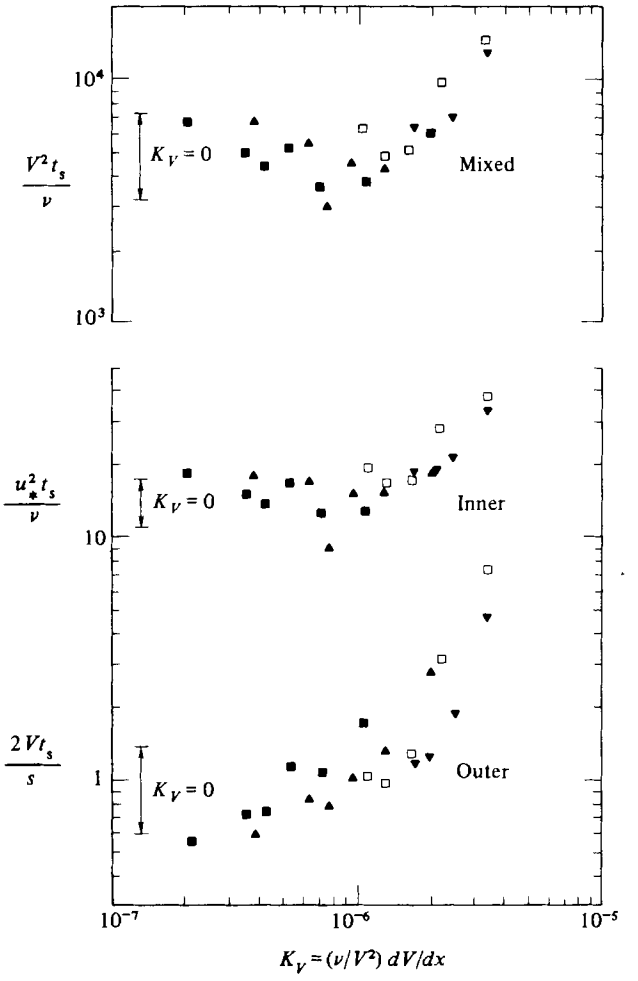

FIGURE 7. Dimensionless sweep times in laterally converging flow; symbols as in figure 5.

Over the range of the present experiments, inner scaling shows less sensitivity to the acceleration parameter. However, both Reynolds number and acceleration parameter are variables on this figure and, for each fixed angle, Re decreases as K_V increases so the reader can gain some further insight into the trends by examining one group at a time.

Since K_V is nominally zero for the fully developed flows, the comparable data of figure 4 cannot be plotted directly on this logarithmic coordinate; however, for convenience, the arrows on the left side of the figure show their range. Alternatively, one can consider the trends of the data for $\theta = 2°$ as primarily representative of the effects of Reynolds number variation, with Re increasing from right to left.

Considering $u_*^2 t_s/\nu$, sweep times scaled by inner variables, one sees the data at $\theta = 2°$ are dominated by the decrease in Re as K_V increases and $u_*^2 t_s/\nu$ decreases, as would be expected from figure 4. The data at $\theta = 8°$ and 16° demonstrate that acceleration tends to increase this non-dimensional sweep time since, despite the decrease in Re with increase in K_V, $u_*^2 t_s/\nu$ increases with K_V. It appears that below $K_V \approx 10^{-6}$ the effect of varying Re is stronger, while above $K_V \approx 2 \times 10^{-6}$ acceleration is dominant. With the exception of one low data point, the measurements

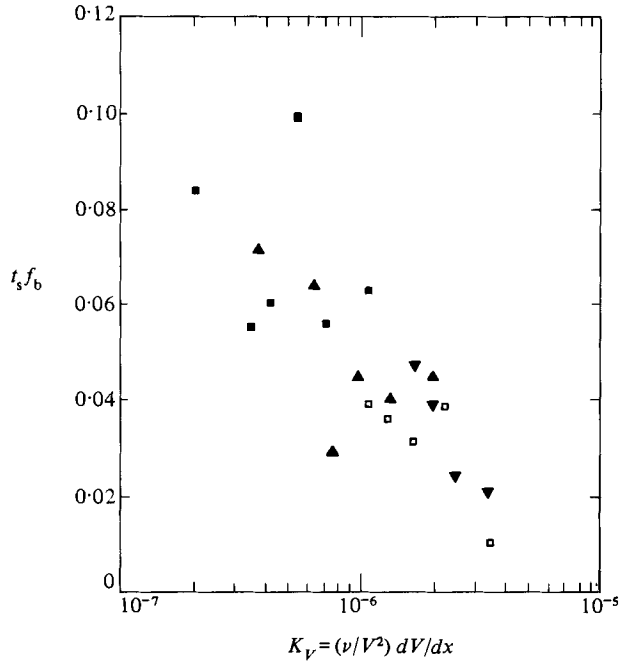

FIGURE 8. Fractional duration of sweep time in laterally converging flow; symbols as in figure 5.

at the intermediate convergence angle of $\theta = 4°$ appear to show the consequences of these competing trends in the vicinity of $K_V = 10^{-6}$; overall $u_*^2 t_s/\nu$ is approximately constant, but below $K_V = 10^{-6}$ a slight decrease may be discerned, and above 10^{-6} the two points increase slightly with K_V.

When presented in terms of mixed scaling these data show the same trends as for inner scaling, both for fully developed and accelerated flows. With outer scaling the trends are different. Figure 4 showed that $2Vt_s/s$ increases as Re decreases; figure 6(*a*) indicates a tendency for $2Vt_s/s$ to increase with K_V at a constant Re. Thus, as K_V is increased at constant θ the two trends reinforce each other to provide the overall pattern, which appears to show a large variation with K_V at the bottom of figure 7.

4.4. *Sweep-time ratio*

An alternative view of the trend from fully turbulent flow to essentially laminar flow as acceleration is increased is provided by examining the product $t_s f_b$. As noted earlier, it is like an intermittency function for the most energetic part of the bursting process, except that its maximum value is not unity but a value of fully turbulent flow (increasing approximately from 0·06 to 0·12 as the Reynolds number increased from 9000 to 47000 for fully developed flow with the present detection scheme and parameters). With a sensitive detection threshold, a value of zero would correspond to effectively laminar flow. Figure 8 presents the burst data in this form.

It will be recalled from part 1 that laminar predictions agreed with mean measurements when K_V was greater than about 4×10^{-6}. The non-dimensional sweep time increases with K_V with each of the three time scalings considered, but from figure 5 it could be seen that the average time between bursts increases even more. Consequently the fraction of time that the sweep event occurs is seen to decrease as K_V increases and appears to extrapolate to zero near $K_V = 4 \times 10^{-6}$. These measurements and the results for bursting frequencies in §4.1 confirm the determination

of effectively laminar flow by the techniques of part 1. Likewise, the intermediate flow regime of part 1 – between fully turbulent and essentially laminar – is seen to correspond to a reduction in this sweep-time ratio and to a reduction in the bursting frequency.

5. Conclusions

Instantaneous measurements of the wall shear stress were made with a flush-mounted heated-filament sensor for flows in which the lateral duct dimension could be adjusted to converge, resulting in acceleration of the flow in the streamwise direction. The sensor was of fixed physical size throughout the experiment. For the 27 flows examined, the Reynolds number based upon hydraulic diameter ranged from 7600 to 47200, and the dimensionless acceleration parameter

$$K_V = \frac{\nu}{V^2}\frac{dV}{dx}$$

ranged from 0 to $3{\cdot}4 \times 10^{-6}$. It was found that a typical burst pattern could be identified by processing the signal via the VITA technique with conditional averaging. This burst pattern found from the wall shear stress resembled that found by Blackwelder & Kaplan (1976) for the streamwise velocity fluctuation at $y^+ = 15$.

For fully developed flows, i.e. flows in which lateral convergence and acceleration were zero, dimensionless bursting frequencies were essentially independent of Reynolds number when scaled with inner variables. Thus, inner scaling was found to be preferable to outer scaling. However, sweep times and magnitudes of the conditionally averaged time histories varied slightly with Reynolds number with either scaling.

For flows accelerating due to lateral convergence, bursting frequencies approached the values for fully developed flow as K_V was reduced towards 10^{-7}, and approached zero as K_V approached 4×10^{-6}, with a continuous variation between these limits. These observations essentially confirm the indications of flow regimes deduced in part 1 by examination of local and integral mean wall parameters.

While acceleration resulted in great decreases in bursting frequency, when scaled in terms of inner or outer variables the sweep time and the time history of the conditionally averaged wall shear stress were less affected. In particular, the sweep pattern remained essentially invariant until K_V approached about 2×10^{-6}, while the non-dimensional bursting frequency dropped considerably after K_V exceeded about 1×10^{-6}. All of the time histories exhibited rapid increases in shear stress followed by slower decays. The sweep time increased, but the ratio of sweep time to average burst period decreased, and the magnitude $\Delta\tau/\tau_{\mathrm{rms}}$ increased slightly as the acceleration parameter increased. These observations were most evident for $K_V \gtrsim 10^{-6}$. As with the effects of Reynolds number in non-accelerated flows, results presented in terms of inner or wall scaling were generally less sensitive to acceleration than those normalized by outer scaling.

Work at the Los Alamos National Laboratory was supported by the U.S. Department of Energy and its predecessors, while work at the University of Arizona was supported by their Engineering Experiment Station and the National Science Foundation. Grateful thanks are expressed to Dr H. Eckelmann and Professors R. F. Blackwelder, F. H. Champagne, W. W. Willmarth, K. R. Sreenivasan, M. T. Landahl and R. L. Simpson for generous advice and constructive criticism at various stages during the study.

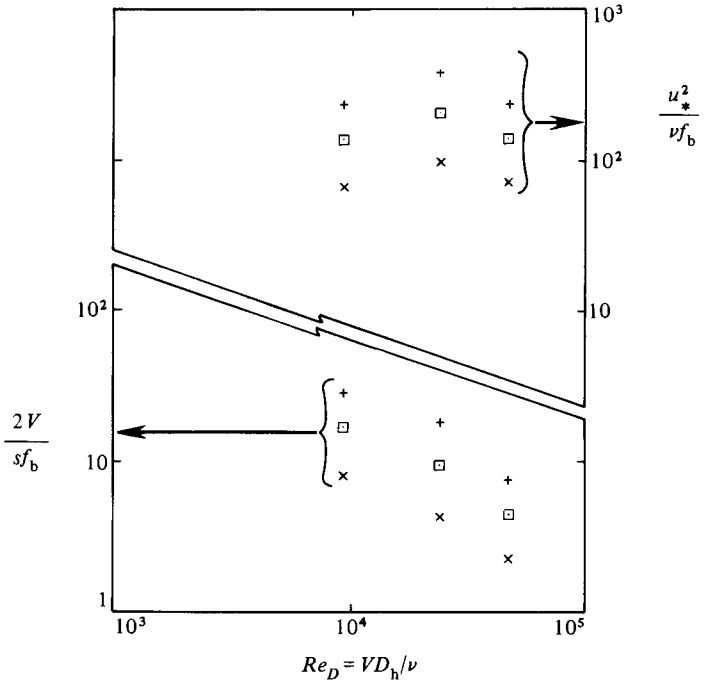

FIGURE 9. Dependence of dimensionless bursting frequencies upon threshold level for fully developed flow: ×, $k = 0{\cdot}15$; ⊡, 0·30; +, 0·45.

Appendix. Threshold-level dependence of bursting frequencies

The results of any conditional analysis of turbulent signals are dependent upon rather arbitrary choices of analysis techniques and the parameters employed in the implementation of these techniques. In the VITA technique of Blackwelder & Kaplan (1976) used in this study, choices of conditional averaging period T and threshold level k must be made. The recommendation of Blackwelder and Kaplan that $Tu_*^2/\nu = 10$ was found to yield averaging times that scaled well with changes in the burst/sweep structure induced by acceleration. That is, the ratio of burst length to T appeared to remain approximately constant. Consequently, their recommendation for T was employed.

However, the threshold level ($k = 1{\cdot}2$) employed by Blackwelder & Kaplan, for a velocity sensor at $y^+ = 15$, was found to detect very few burst events in the signal trace of the flush-mounted shear-stress sensor used in the present study. As previously discussed, the choice of k is quite subjective, and different values of it yield different bursting frequencies. The choice of $k = 0{\cdot}3$ was made by having three separate observers examine the entire trace of a high-Reynolds-number zero-acceleration flow and count the number of burst events that were apparent to them. A similar procedure was followed by Crow & Champagne (1971) when detecting large-scale structures in round jets from flow-visualization ciné films. The basic criterion used by the observers in this study was that, when an event occurs, the shear stress should enhibit a very rapid and strong increase followed by a slow decrease. It was found that analysis using a value of $k = 0{\cdot}3$ resulted in a number of burst detections close to the average number counted by the three observers.

While the bursting frequencies reported do depend upon the value of k employed, it is believed that the trends reported in this work are independent of the value of

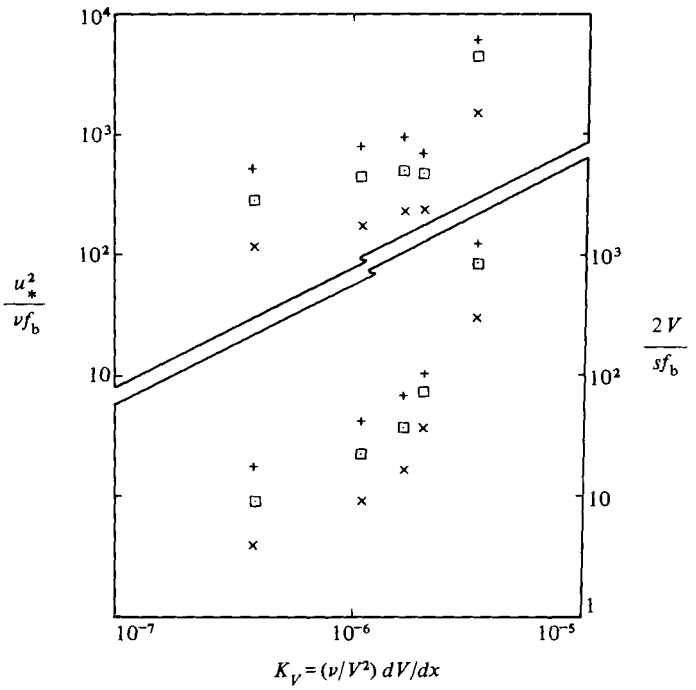

FIGURE 10. Dependence of dimensionless bursting frequencies upon threshold level for laterally converging flow; symbols as in figure 9.

k. A test of the dependence of these trends upon the threshold level was performed by analysing eight runs using threshold levels of $k = 0{\cdot}15$, $0{\cdot}30$ and $0{\cdot}45$. The resulting non-dimensionalized burst frequencies are presented in figure 9 for fully developed flow cases and in figure 10 for accelerating-flow cases. The same trends are apparent for each value of k. Thus one may conclude that the trends reported here are not dependent upon the parameter values employed in the conditional-analysis scheme.

REFERENCES

BLACK, T. J. 1966 Some practical applications of a new theory of wall turbulence. In *Proc. Heat Transfer and Fluid Mech. Inst.*, pp. 366–386. Stanford University Press.

BLACK, T. J. 1968 An analytical study of the measured wall pressure field under supersonic turbulent boundary layers. *NASA* CR-888.

BLACKWELDER, R. F. 1978 Fortran listing of VITA program (University of Southern California, unpublished manuscript).

BLACKWELDER, R. F. & ECKELMANN, H. 1978 The spanwise structure of the bursting phenomenon. In *Structure and Mechanisms of Turbulence I* (ed. H. Fiedler). Lecture Notes in Physics, vol. 75, pp. 190–204. Springer.

BLACKWELDER, R. F. & HARITONIDIS, J. H. 1980 Reynolds number dependence of the bursting frequency in turbulent boundary layers. *A.P.S. Meeting, Ithaca, N.Y.*

BLACKWELDER, R. F. & HARITONIDIS, J. H. 1981 The bursting frequency in turbulent boundary layers (unpublished manuscript).

BLACKWELDER, R. F. & KAPLAN, R. E. 1976 On the wall structure of the turbulent boundary layer. *J. Fluid Mech.* **76**, 89–112.

BLACKWELDER, R. F. & KOVASZNAY, L. S. G. 1972 Large scale motion of a turbulent boundary-layer during relaminarization. *J. Fluid Mech.* **53**, 61–83.

BROWN, G. L. & THOMAS, A. S. W. 1977 Large structure in a turbulent boundary layer. *Phys. Fluids Suppl.* **20**, S243–S252.

CANTWELL, B. 1981 Organized motion in turbulent flow. *Ann. Rev. Fluid Mech.* **13**, 457–515.

CHAMBERS, F. W. & MURPHY, H. D. 1981 Turbulent wall shear stress fluctuations in fully developed and accelerating flows. *Los Alamos Natl Lab. Tech. Rep.* LA-8781-MS.

CORINO, E. R. & BRODKEY, R. S. 1969 A visual observation of the wall region in turbulent flow. *J. Fluid Mech.* **37**, 1–30.

CROW, S. C. & CHAMPAGNE, F. H. 1971 Orderly structure in jet turbulence. *J. Fluid Mech.* **48**, 547–591.

ECKELMANN, H. 1974 The structure of the viscous sublayer and the adjacent wall region in a turbulent channel flow. *J. Fluid Mech.* **65**, 439–459.

JONES, W. C. & LAUNDER, B. E. 1972 Some properties of sink-flow turbulent boundary layers. *J. Fluid Mech.* **56**, 337–351.

KIM, H. T., KLINE, S. J. & REYNOLDS, W. C. 1971 The production of turbulence near a smooth wall in the turbulent boundary layer. *J. Fluid Mech.* **50**, 133–160.

KLINE, S. J., REYNOLDS, W. C., SCHRAUB, F. A. & RUNDSTADLER, P. W. 1967 The structure of turbulent boundary layers. *J. Fluid Mech.* **30**, 741–773.

LANDAHL, M. T. 1980 A theoretical model for coherent structures in wall turbulence. *ICHM/IUTAM Meeting, Dubrovnik, October* 1980.

MCELIGOT, D. M. 1963 Effect of large temperature gradients on turbulent flow of gases in the downstream region of tubes. PhD thesis, Stanford University.

MCELIGOT, D. M. & MURPHY, H. D. 1978 Turbulent flow in a spanwise converging duct. *A.P.S. Meeting, Los Angeles.*

MORETTI, P. M. & KAYS, W. M. 1965 Heat transfer to a turbulent boundary layer with varying free stream velocity and varying surface temperature. *Int. J. Heat Mass Transfer* **8**, 1187–1202.

MURPHY, H. D. 1979 Flow near the outlet of a geothermal energy reservoir. PhD thesis, University of Arizona.

MURPHY, H. D., CHAMBERS, F. W. & MCELIGOT, D. M. 1983 Laterally converging flow. Part 1. Mean flow. *J. Fluid Mech.* **127**, 379–401.

NARASIMHA, R. & SREENIVASAN, K. R. 1973 Relaminarization in highly accelerated turbulent boundary layers. *J. Fluid Mech.* **61**, 417–447.

NARASIMHA, R. & SREENIVASAN, K. R. 1979 Relaminarization of fluid flows. *Adv. Appl. Mech.* **19**, 221–309.

OFFEN, G. R. & KLINE, S. J. 1974 Combined dye-streak and hydrogen-bubble visual observations of a turbulent boundary layer. *J. Fluid Mech.* **62**, 223–239.

RAO, K. N., NARASIMHA, R. & BADRI NARAYANAN, M. A. 1971 The 'bursting' phenomena in a turbulent boundary layer. *J. Fluid Mech.* **48**, 339–352.

SCHUBERT, G. & CORCOS, G. M. 1967 The dynamics of turbulence near a wall according to a linear model. *J. Fluid Mech.* **29**, 113–135.

SHARMA, L. K. & WILLMARTH, W. W. 1980 Study of turbulent structure with hot wires smaller than the viscous length. University of Michigan, manuscript in preparation.

SIMPSON, R. L. 1976 An investigation of the spatial structure of the viscous layer. *Max-Planck-Inst. f. Strömungsforschung, Bericht* 118/1976.

SIMPSON, R. L. 1979 Some features of strongly accelerated turbulent boundary layers. In *Proc. 2nd Int. Symp. Turb. Shear Flow, London.*

SIMPSON, R. L. & WALLACE, D. B. 1975 Laminarescent turbulent boundary layers: experiments on sink flows. *Project Squid Techn. Rep. SMU-1-PU, Thermal Science and Propulsion Center, Purdue University.*

STRICKLAND, J. H. 1973 The separating turbulent boundary layer: an experimental study of an airfoil-type flow. PhD thesis, Southern Methodist University.

STRICKLAND, J. H. & SIMPSON, R. L. 1975 'Bursting' frequencies obtained from wall shear stress fluctuations in a turbulent boundary layer. *Phys. Fluids* **18**, 306–308.

SREENIVASAN, K. R., PRABHU, A. & NARASIMHA, R. 1982 Zero-crossings in turbulent signals (unpublished manuscript).

WALLACE, J. H., BRODKEY, R. S. & ECKELMANN, H. 1977 Pattern-recognized structures in bounded turbulent shear flows. *J. Fluid Mech.* **83**, 673–693.

WILLMARTH, W. W. 1975 Structure of turbulence in boundary layers. *Adv. Appl. Mech.* **15**, 159–254.

WILLMARTH, W. W. & LU, S. S. 1971 Structure of the Reynolds stress near the wall. *AGARD Conf. Proc.* 93: *Turbulent shear flow, London*, 13–15 *September*.

ZAKKAY, V., BARRA, V. & HOZUMI, K. 1979 Turbulent boundary layer structure at low and high subsonic speeds. *AGARD Conf. Preprint* 271: *Turbulent Boundary Layers – Experiments, Theory and Modelling, The Hague*, 24–26 *September*, pp. 4-1–4-20.